Bioelectrochemistry 74 (2008) 130–141

Contents lists available at ScienceDirect

Bioelectrochemistry

journal homepage: www.elsevier.com/locate/bioelechem

Effects of cell orientation and electric field frequency on the transmembrane potential induced in ellipsoidal cells

Kanokkan Maswiwat [a], Derk Wachner [b], Jan Gimsa [b,*]

[a] Department of Physics, Faculty of Science and Technology, Suratthani Rajabhat University, 84100, Suratthani, Thailand
[b] Chair of Biophysics, Institute of Biology, University of Rostock, Gertrudenstr. 11a, 18057, Rostock, Germany

ARTICLE INFO

Article history:
Received 28 November 2007
Received in revised form 22 May 2008
Accepted 2 June 2008
Available online 5 June 2008

Keywords:
Induced transmembrane potential
Electroporation
Electropermeabilization
Lab-on-chip
Chicken red blood cells

ABSTRACT

The transmembrane potential ($\Delta\phi$) induced by external electric fields is important both in biotech applications and in new medical therapies. We analyzed the effects of AC field frequency and cell orientation for cells of a general ellipsoidal shape. Simplified equations were derived for the membrane surface points where the maximum $\Delta\phi$ is induced. The theoretical results were confirmed in experiments with three-axial chicken red blood cells (a:b:c=6.66 μm:4.17 μm:1.43 μm). Propidium iodide (PI) staining and cell lysis were detected after an AC electropermeabilization (EP) pulse. The critical field strength for both effects increased when the shorter axis of a cell was parallel to the field, as well as at higher field frequency and for shorter pulse durations. Nevertheless, data analysis based on our theoretical description revealed that the $\Delta\phi$ required is lower for the shorter axis, i.e. for smaller membrane curvatures. The critical $\Delta\phi$ was independent of the field frequency for a given axis, i.e. the field strength had to be increased with frequency to compensate for the membrane dispersion effect. Comparison of the critical field strengths of PI staining in a linear field aligned along semi-axis a (142 kV m^{-1}) and a field rotating in the a–b plane (115 kV m^{-1}) revealed the higher EP efficiency of rotating fields.

1. Introduction

Membrane electropermeabilization (EP, also referred to as electroporation or dielectric breakdown) is probably the most important technique for the introduction of extracellular molecules, which do not penetrate cell membranes under normal conditions. It is generally assumed that membrane re-conformation and the formation of aqueous pores play a decisive role in the process of penetration [1]. EP is observed when the transmembrane potential ($\Delta\phi$) induced by the external field reaches a "critical voltage" of approximately 1 V [2–4]. Its magnitude depends on the experimental conditions [5,6]. Nevertheless, thorough investigations have shown that the experimental observation of a "critical voltage" results from the strongly nonlinear auto-regulation processes involved in pore formation [7–9]. One important effect is the voltage drop in the external medium for the current flowing through the pore. This voltage drop increases with pore size, leading to a down-regulation of $\Delta\phi$. Nevertheless, the assumption of a "critical voltage" is feasible for practical reasons and we will use the term in the following.

EP of cells depends on several electric parameters, e.g. field strength, pulse duration, number of pulses [6,10–17] and pulse shape [18–20]. Cell size, shape and orientation, medium conductivity and temperature are also important [6,21–23]. $\Delta\phi$ is proportional to the length of the axis oriented in the field direction and a shape factor that is related to the depolarizing factors [24–25]. Chang et al. [26] described how AC-fields are more effective in EP than DC fields, and result in an increased cell viability. The frequency dependence of $\Delta\phi$ in AC-fields depends on medium conductivity [22]. Capacitive membrane bridging causes the $\Delta\phi$ to decrease with increasing field frequency [4,22,27–34]. Clearly, rotating AC-fields generated by the superposition of two perpendicularly oriented fields are even more effective than the linear AC-fields [28,35,36].

New developments focus on EP in microfluidic devices with an EP process controlled at the single cell level [37,38]. The aims are to achieve high effectiveness in the genetic manipulation of cells [39–43] and effective cell lysis prior to subcellular analysis [44].

Gimsa and Wachner [25,45] have derived analytical expressions of $\Delta\phi$ for both orientations of the symmetry axis of spheroidal cells, assuming a low conductive membrane and a highly polarizable cytoplasm. The same ansatz could be extended to arbitrarily oriented cells of the general ellipsoidal shape, including all electrical parameters [30]. Recently, we derived simplified expressions avoiding the complex depolarizing factors for spheroidal cells [46].

In this work, we analyze the $\Delta\phi$ induced by AC field pulses in arbitrarily oriented ellipsoidal cells. The theoretical description is compared to experimental results obtained from the EP of the roughly ellipsoidal chicken red blood cells (CRBCs). Experiments were conducted

* Corresponding author. Tel.: +49 381 498 6020; fax: +49 381 498 6022.
E-mail address: jan.gimsa@uni-rostock.de (J. Gimsa).

1567-5394/$ – see front matter © 2008 Elsevier B.V. All rights reserved.
doi:10.1016/j.bioelechem.2008.06.001

in a chip chamber with two comb-shaped electrodes. Each comb had three interdigitating fingers, allowing for five different inter-electrode distances. The EP of the cells was determined from the two criteria, propidium iodide (PI) permeabilization detected by fluorescence-staining of the cell nuclei and cell lysis, respectively. We considered the effects of field strength, pulse field frequency, pulse duration and cell orientation.

2. Theory

2.1. $\Delta\phi$ for general orientation of ellipsoidal cells

2.1.1. A finite element ansatz for $\Delta\phi$ of the oriented single shell model

Gimsa and Wachner [30] have presented a simplified finite element ansatz for the $\Delta\phi$ of a single shell ellipsoidal model. The model consists of the internal, membrane and external media, designated by the indices *i*, *m* and *e*, respectively. Each medium is presented by a prismatic element (see [30]). The impedance Z^* of each element is given by the geometry (cross-sectional area *A* and length *l*):

$$Z^* = \frac{1}{\sigma^* A} l \text{ with } \sigma^* = \sigma + j\omega\varepsilon\varepsilon_0 \tag{1}$$

σ^*, ε, ε_0 and *j* stand for the complex specific conductivity of the considered medium, relative permittivity, permittivity of vacuum and $\sqrt{-1}$, respectively. Eq. (1) is equivalent to a resistor capacitor- (RC-) pair (see lump model in [30]). The length l in Eq. (1) is given by the dimensions. The cross-sectional areas A of each element are assumed to be equal and infinitely small. They are oriented perpendicular to the field. Starting from this "finite element model", for an ellipsoidal cell with semiaxis a oriented in parallel to the field direction $\Delta\phi$ at pole a can be expressed by the voltage divider properties of the lump model (see [30] for details):

$$\begin{aligned}\Delta\phi_a &= -a\left(E_{\mathrm{loc},a} - E_{i,a}\right) = -\frac{\left(Z^*_{i,a}+Z^*_m\right)\phi_a^{\max}}{Z^*_{i,a}+Z^*_m+Z^*_{e,a}} + \frac{Z^*_{i,a}\phi_a^{\max}}{Z^*_{i,a}+Z^*_m+Z^*_{e,a}} \\ &= \frac{-Z^*_m}{Z^*_{i,a}+Z^*_m+Z^*_{e,a}} a_{\mathrm{infl}} E_x\end{aligned} \tag{2}$$

E_x, $E_{\mathrm{loc},a}$ and $E_{i,a}$ stand for the external field in *x*-direction, the effective internal local field of the body and the cytoplasmic field, respectively. Please note that $\Delta\phi_a$, $E_{\mathrm{loc},a}$ and $E_{i,a}$ are complex terms. Nevertheless, for simplicity we only mark the impedances Z^* of the prismatic elements by asterisks. $\phi_a^{\max}$ stands for the maximum of $\phi_{\mathrm{loc},a}$ determined by the influential radius a_{infl} along axis *a*. Index *a* refers to the geometry along semiaxis *a*. No axis index is required for the membrane impedance because the membrane elements are assumed to possess the same geometry along each principal axis. Please note that the model is largely consistent with (or even superior over) the Laplace-description for reasonable cell properties [30].

2.1.2. $\Delta\phi$ for arbitrarily oriented cells of the general ellipsoidal shape

The general ellipsoidal model is described by three principal semiaxes *a*, *b*, and *c* of different length. Special cases are spheroidal models with $a=b$ and spherical ones with $a=b=c$. The semi-axes can be used to determine a Cartesian, orthonormal coordinate system *x*, *y*, and *z* where *x*, *y*, and *z* are parallel to *a*, *b*, and *c*, respectively (Fig. 1). The homogeneous external field $\boldsymbol{E}$ is oriented arbitrarily within this coordinate system. Its orientation is determined by the angles δ and γ. The local vector $\boldsymbol{P}$ of the membrane point under consideration is determined by the angles α and β. The induced transmembrane potential ($\Delta\phi_p$) at a membrane point (index *p*) is:

$$\Delta\phi_p = \begin{pmatrix} \frac{-Z^*_m}{Z^*_{i,a}+Z^*_m+Z^*_{e,a}} \frac{a_{\mathrm{infl}}}{a} d_x E_x \\ \frac{-Z^*_m}{Z^*_{i,b}+Z^*_m+Z^*_{e,b}} \frac{b_{\mathrm{infl}}}{b} d_y E_y \\ \frac{-Z^*_m}{Z^*_{i,c}+Z^*_m+Z^*_{e,c}} \frac{c_{\mathrm{infl}}}{c} d_z E_z \end{pmatrix} = \begin{pmatrix} \frac{d_x}{a}\Delta\phi^*_a \\ \frac{d_y}{b}\Delta\phi^*_b \\ \frac{d_z}{c}\Delta\phi^*_c \end{pmatrix} \tag{3}$$

for an arbitrary orientation of the inducing field (see [30] for details). a_{infl}, b_{infl} and c_{infl} stand for the influential radii of the ellipsoidal cell along the three semiaxes. Again, all $\Delta\phi$-terms are complex. The influential radius along each semiaxis refers to a certain distance from the center of the cell [45]. In the center, a symmetry plane can be defined for each semiaxis that is oriented perpendicular to the semiaxis. Field components (E_x, E_y, E_z) parallel to a semiaxis will not change the potential in the respective symmetry plane for symmetry reasons. The $\Delta\phi$-components at the three poles *a*, *b*, and *c* are solely induced by the respective field components (E_x, E_y, E_z) along the semiaxes. d_x, d_y, and d_z denote the distance of the membrane point to the three symmetry planes. At the poles $d_x=a$, $d_y=b$, and $d_z=c$. For a cytoplasmic conductivity much higher than the membrane conductivity and a very thin membrane, $\Delta\phi_p$ is given by the sum of the vector components of Eq. (3) (see [30] for a detailed consideration). Neglecting the permittivities of the cytoplasm and the external medium, from Eq. (3) we obtain [30]:

$$\begin{aligned}\Delta\phi_p = &\frac{-a_{\mathrm{infl}}E_x d_x/a}{\left(1+ag_m\left(1/\sigma_i+(a_{\mathrm{infl}}-a)/a\sigma_e\right)\right)\sqrt{1+f^2/f^2_{c,a}}} \\ &+\frac{-b_{\mathrm{infl}}E_y d_y/b}{\left(1+bg_m\left(1/\sigma_i+(b_{\mathrm{infl}}-b)/b\sigma_e\right)\right)\sqrt{1+f^2/f^2_{c,b}}} \\ &+\frac{-c_{\mathrm{infl}}E_z d_z/c}{\left(1+cg_m\left(1/\sigma_i+(c_{\mathrm{infl}}-c)/c\sigma_e\right)\right)\sqrt{1+f^2/f^2_{c,c}}}\end{aligned} \tag{4}$$

with

$$f_{c,a} = \frac{1}{2\pi C_m}\left(\frac{\sigma_e\sigma_i}{a\sigma_e+(a_{\mathrm{infl}}-a)\sigma_i}+g_m\right) \tag{5}$$

C_m and g_m stand for the area-specific membrane capacitance in Fm^{-2} and the area-specific membrane conductance in Sm^{-2}, respectively. They are given by $C_m=\varepsilon_0\varepsilon_m/d$ and $g_m=\sigma_m/d$ with *d* being the membrane thickness. *f*, $f_{c,a}$, σ_i, and σ_e stand for the external field frequency, the characteristic frequency of membrane polarization along semiaxis *a*, and the internal and external conductivities, respectively. Expressions analogous to Eq. (5) hold along the other two semiaxes.

2.1.3. Maximum of $\Delta\phi_p$ for semiaxis b being oriented perpendicular to the external field

The field vector is parallel to the *x*–*z* plane for semiaxis *b* being orientated perpendicular to the external field ($\delta=0°$, Fig. 2A). A new analytical expression can be derived from Eq. (3) for the membrane surface point reaching the maximum $\Delta\phi$ if only peripheral points in the *a*–*c* plane ($\beta=0°$) are considered. The angle $\alpha_{(\Delta\phi^{\max})}$ determining this point can be obtained considering the α-dependence of the sum of the *x*- and *z*-components of Eq. (3) (compare to Eq. (4)). The α-dependence of Eq. (3) is obtained after introduction of angular coordinates for the distances d_x, d_y, and d_z (see [30] and compare to

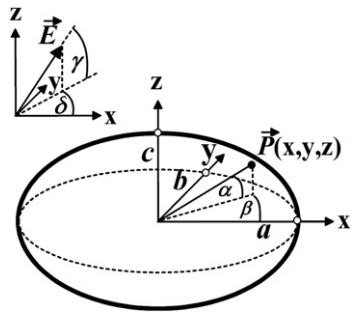

Fig. 1. Sketch of a cell of the general ellipsoidal shape. The components of *P* and *E* are given in spherical coordinates. The principal semiaxes *a*, *b* and *c* define the orthonormal coordinate system, *x*, *y* and *z*. *P* (*x*, *y*, *z*) is the local vector of a membrane surface point defined by the angles α and β. The external electric field *E* has an arbitrary orientation, determined by the angles δ and γ.

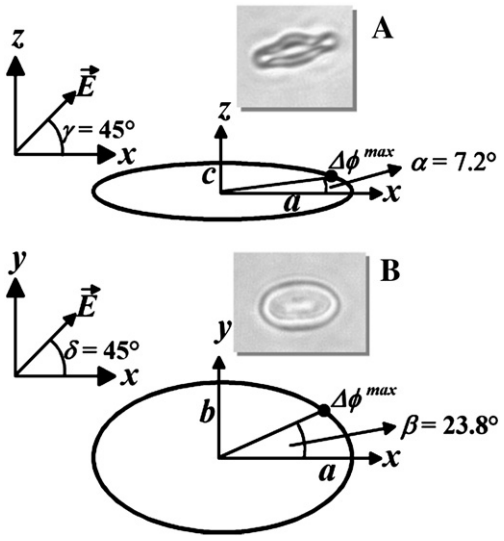

Fig. 2. Two-dimensional sketches of the ellipsoidal CRBC model compared to microscopic images of CRBCs in the measuring solution. The sketches resemble a situation of a 45° field orientation in the *a*–*c* (A) and *a*–*b* (B) planes ($\delta=\gamma=45°$). α and β determine the theoretical membrane points of $\Delta\phi^{max}$. (A) field orientation perpendicular to semiaxis *b* ($\delta=0°$). (B) experimental standard situation, field orientation perpendicular to the shortest semiaxis *c* ($\gamma=0°$, compare to Fig. 10).

Eq. (9)). Assuming the first derivative of the obtained function to be zero for $|E_x|=|E_z|$ and $|E_y|=0$, i.e. $\gamma=45°$ and $\delta=0°$ we obtain:

$$\alpha_{(\Delta\phi^{max})} = \arctan\left(\frac{|\Delta\phi_c^*|c}{|\Delta\phi_a^*|a}\tan\gamma\right) \tag{6}$$

Introducing $\alpha_{(\Delta\phi^{max})}$ into Eq. (3) leads to the maximum of $\Delta\phi$:

$$\Delta\phi^{max} = \sqrt{|\Delta\phi_a^*|^2\cos^2\gamma + |\Delta\phi_c^*|^2\sin^2\gamma} \tag{7}$$

Analogous expressions hold for fields oriented in the *x*-*y* and *y*-*z* planes. In these cases, the field orientation and the membrane point under consideration will be defined by the angles δ and β, respectively (Fig. 2B). Similarly, also other field orientations can be considered. An interesting consideration is the frequency dependence of the $\Delta\phi^{max}$ point for $\gamma=\delta=45°$. In this case, the site of $\Delta\phi^{max}$ will exhibit a complex frequency-dependent trajectory at the membrane surface.

2.2. DC-limit of $\Delta\phi_p$ for oriented ellipsoidal cells with zero membrane conductance

2.2.1. General orientation of a cell of the general ellipsoidal shape

For zero membrane conductance and at very low frequency or DC fields, Eq. (3) can be reduced to:

$$\Delta\phi_p = \begin{pmatrix} \frac{d_x}{a}\Delta\phi_a^* \\ \frac{d_y}{b}\Delta\phi_b^* \\ \frac{d_z}{c}\Delta\phi_c^* \end{pmatrix} = \begin{pmatrix} \frac{-d_x a_{infl}}{a}E_x \\ \frac{-d_y b_{infl}}{b}E_y \\ \frac{-d_z c_{infl}}{c}E_z \end{pmatrix} \tag{8}$$

After introduction of angular coordinates for the distances d_x, d_y, and d_z (see [30]) into Eq. (3) we obtain:

$$\Delta\phi_p = \frac{-E\,abc}{\sqrt{\left(a^2\sin^2\beta + b^2\cos^2\beta\right)c^2\cos^2\alpha + a^2b^2\sin^2\alpha}} \times \begin{pmatrix} a_{infl}\cos\alpha\cos\beta/a \\ b_{infl}\cos\alpha\sin\beta/b \\ c_{infl}\sin\alpha/c \end{pmatrix}\begin{pmatrix} \cos\gamma\cos\delta \\ \cos\gamma\sin\delta \\ \sin\gamma \end{pmatrix} \tag{9}$$

2.2.2. $\Delta\phi_p$ for a perpendicular orientation of semiaxis b to the external field

For semiaxis *b* being oriented perpendicular to the external field, Eq. (9) can be reduced to:

$$\Delta\phi_p = \frac{-E(a_{infl}\,c\,\cos\gamma\,\cos\alpha + c_{infl}\,a\sin\gamma\sin\alpha)}{\sqrt{a^2\sin^2\alpha + c^2\cos^2\alpha}} \tag{10}$$

considering only peripheral points in the *a*–*c* plane (Fig. 2A). The angle $\alpha_{(\Delta\phi^{max})}$ determining $\Delta\phi^{max}$ is given by (compare to Eq. (6)):

$$\alpha_{(\Delta\phi^{max})} = \arctan\left(\frac{c_{infl}c}{a_{infl}a}\tan\gamma\right) \tag{11}$$

and after introducing $\alpha_{(\Delta\phi^{max})}$ into Eq. (10) we obtain (compare to Eq. (7)):

$$\Delta\phi^{max} = -E\sqrt{a_{infl}^2\cos^2\gamma + c_{infl}^2\sin^2\gamma} \tag{12}$$

Eqs. (11) and (12) indicate that the $\Delta\phi^{max}$ of ellipsoidal cells for the above simplifications depends on field orientation (γ) and cell shape, i.e. the influential radii along semiaxes *a* and *c* (Fig. 2A). Analogous expressions hold for the peripheral points of the *a*–*b* (Fig. 2B) and *b*–*c* planes.

2.3. DC-limit of $\Delta\phi_p$ for spheroidal cells with zero membrane conductance

2.3.1. General orientation of a spheroidal cell

Spheroidal models are oblate and prolate when their symmetry axes are shorter ($c<a=b$) and longer ($c>a=b$) than the semiaxes *a* and *b*, respectively. For arbitrarily oriented spheroidal cells $\Delta\phi_p$ is given by [45]:

$$\Delta\phi_p = -\frac{a_{infl}}{a}(E_x d_x + E_y d_y) - \frac{c_{infl}}{c}E_z d_z \tag{13}$$

From Eq. (9) we obtain:

$$\Delta\phi_p = \frac{-E\,ac}{\sqrt{\left(a^2\sin^2\alpha + c^2\cos^2\alpha\right)}} \begin{pmatrix} a_{infl}\cos\alpha\,\cos\beta/a \\ a_{infl}\cos\alpha\,\sin\beta/a \\ c_{infl}\,\sin\alpha/c \end{pmatrix}\begin{pmatrix} \cos\gamma\cos\delta \\ \cos\gamma\sin\delta \\ \sin\gamma \end{pmatrix} \tag{14}$$

2.3.2. $\Delta\phi_p$ at peripheral membrane points with a perpendicular orientation of semiaxes b to the external field for a spheroidal cell

For $\delta=0°$ the field vector lies in *x*–*z* plane. If we further assume $\beta=0°$, $\Delta\phi_p$ in Eq. (9) can be reduced to Eq. (10). Nevertheless, a_{infl} and c_{infl} are based on complex expressions for the depolarizing factors [45]. Recently, we derived simple approximating equations for a_{infl} and c_{infl} of spheroids avoiding complex expressions (see Appendix A). Introducing Eqs. (A.1) and (A.2) into Eq. (10) leads to:

$$\Delta\phi_p = -\frac{a\,E(a+2c)(2c\cos\gamma\cos\alpha + (a+c)\sin\gamma\,\sin\alpha)}{2(a+c)\sqrt{a^2\sin^2\alpha + c^2\cos^2\alpha}} \tag{15}$$

The same expressions can be introduced into Eqs. (11) and (12) to determine the $\Delta\phi^{max}$ and the angle $\alpha_{(\Delta\phi^{max})}$ under which it occurs. Furthermore, limiting cases of the shape can be considered. For a thin disk ($c\ll a$) Eq. (15) reduces to:

$$\Delta\phi_p = -\frac{a\,E(2c\cos\gamma\cos\alpha + a\sin\gamma\,\sin\alpha)}{2\sqrt{a^2\sin^2\alpha + c^2\cos^2\alpha}} \tag{16}$$

Table 1
CRBC parameters for model calculations [47]

Parameter	Value
Infl. radius/semiaxis=max. ampl. factor	
a_{infl} / a	7.49 µm/6.66 µm=1.125
b_{infl} / b	5.28 µm/4.17 µm=1.266
c_{infl} / c	4.43 µm/1.43 µm=3.098
Membrane thickness (d)	8 nm
Conductivity/relative permittivity	
Internal: σ_i /ε_i	0.36 S m^{-1}/50
Membrane: σ_m/ε_m	28 µS m^{-1}/22.59
External: σ_e/ε_e	0.12 S m^{-1}/78.5
Area specific membrane conductance (g_m)	3500 S m^{-2}
Area specific membrane capacitance (C_m)	0.025 Fm^{-2}

The influential radii were calculated from the depolarizing factors of general ellipsoids [30]. The quotient of influential radius and semiaxes length is the maximal amplification factor for the induced $\Delta\phi$.

For long cylindrical cells ($c \gg a$), $\Delta\phi_p$ becomes:

$$\Delta\phi_p = -\frac{a\,c\,E(2\cos\gamma\cos\alpha + \sin\gamma\sin\alpha)}{\sqrt{a^2\sin^2\alpha + c^2\cos^2\alpha}} \quad (17)$$

2.3.3. $\Delta\phi_p$ for peripheral membrane points of a spheroidal cell for a perpendicular orientation of symmetry axis c to the field

δ is equal to $\beta_{(\Delta\phi^{max})}$ for any γ because of the axis-symmetry of spheroids. For γ=0°, the field vector is parallel to the x–y plane. The peripheral points of spheroids (a=b) form circles in this plane, i.e. for α=0°, $\Delta\phi_a^{max}$ is always given by a_{infl} E. Using Eq. (A.1) we obtain [46]:

$$|\Delta\phi_a^{max}| = aE\left(\frac{a+2c}{a+c}\right) \quad (18)$$

For the limiting case of a very thin disk ($c \ll a$), Eq. (18) becomes $|\Delta\phi_a^{max}| = aE$. For an extreme prolate shape ($c \gg a$), the geometry approaches a cylinder and $|\Delta\phi_c^{max}| = 2aE$.

3. Experimental

3.1. Theoretical analysis of the model behavior

We used Maple 9.5 (Maplesoft, Waterloo Maple Inc., Canada) for calculations. Curves were plotted with SigmaPlot 9.0 (Systat Software GmbH, Germany). The cells were modeled as general single shell ellipsoids (a>b>c), spheres (a=b=c) and oblate (c<a=b) or prolate (c>a=b) spheroids. An electric field strength of 100 kV m^{-1} was assumed for theoretical considerations. Electric CRBC parameters are given in Table 1. In experiments, a sufficient number of cells could only be found with the orientation γ=0°, α=0° (Fig. 2B). The orientation δ=0°, β=0° was not stable enough for reliable data analysis (Fig. 2A).

3.2. Electropermeabilization (EP) experiments

3.2.1. EP chip chamber and instrumentation

A glass chip with two comb-shaped platinum electrodes with three fingers was used for EP experiments. Our new design allowed for five different inter-electrode gaps of 80 µm, 100 µm, 150 µm, 300 µm and 450 µm generating five electric field strengths from the same supply voltage (Fig. 3). The chips were fabricated by GeSiM GmbH, Grosserkmannsdorf, Germany (www.gesim.de). Only the three shortest distances (80 µm, 100 µm and 150 µm) were used in the CRBC experiments. The AC fields were generated by two 180°-phase shifted square-topped signals with a key ratio of 1:1 from a function generator HP 8130A (Hewlett Packard GmbH, Germany). The parameters of the generator were controlled by a computer program. The output voltage could be amplified up to 20 V_{pp} at frequencies up to 60 MHz by a home made amplifier. A pulse generator HP 8116A (Hewlett Packard GmbH, Germany) was used to generate the gating signal for the HP 8130A function generator. Waveform and amplitude of the AC-fields were monitored with an oscilloscope HP 54610B (Hewlett Packard GmbH, Germany). The resistances of the on-chip temperature sensors were calibrated for their temperature dependencies and measured before and after pulse application by a multimeter (model 2000, Keithley Instruments Inc., USA).

After the EP pulse, a short temperature increase has been observed with a maximum of 0.9 degrees for the longest pulse duration of 200 ms. The temperature peak was observed approx. 50 s after the pulse. The main reason for this behavior was the heat dissipation by the terminating resistors. The temperature approached room temperature approx. one minute after the peak.

3.2.2. Electric field in the chamber

The electric field strength (E) is given by a Fourier series for a square-wave AC-pulse with a key ratio of 1:1 [36]:

$$E = \frac{4V_{ss}}{\pi d}[\exp(j\omega t) - \exp(-j3\omega t)/3 + \exp(j5\omega t)/5 - \ldots + \ldots] \quad (19)$$

d, V_{ss}, j, ω and t stand for the distance of a pair of plane-parallel electrodes, the voltage difference between the electrodes, $\sqrt{-1}$, the circular frequency, and time, respectively. The Fourier series contains only odd harmonics. While the effective field of the full series is V_{ss}/d, the effective field generated by the sinusoidal first harmonic is $2\sqrt{2}V_{ss}/(\pi d)$ leaving a missing 9.94% contribution for all other harmonics of the series. The missing contribution decreases to 5.05% and 3.36% when the third and fifth harmonics are included in the series. This consideration might be interesting in the frequency range of membrane dispersion when capacitive membrane bridging reduces the induced transmembrane potential with increasing frequency, i.e. membrane dispersion leads to a relatively stronger decrease in the contributions of the higher harmonics.

3.2.3. Cells and sample preparations

CRBCs were chosen because of their 3-axial ellipsoidal shape. Fig. 4 presents micrographs of the cells (Scanning Electron Microscope, DSM 960A, Carl Zeiss, Oberkochen, Germany).

The cells were obtained from the BfR (Bundesinsitut für Risikobewertung, Berlin, Germany). Fresh blood samples taken from the wing vein of Italian cocks were preserved at a 1:1 dilution in Alsever's solution (18.66 g dextrose, 4.18 g NaCl and 8.0 g tri-Na-citrate-2-hydrate dissolved in 1 liter distilled water, pH 6.1) as an anticoagulant. This suspension had a cell concentration of approx. 19% *v/v*. It was stored no longer than three days. Cells were suspended in a mixture of a sucrose and a NaCl solution for experiments. Both solutions had an osmolarity of 300 mOsm and contained 1 mM phosphate buffer solution, pH 6.8. The mixture was adjusted to a medium conductivity of 0.12 S/m. The

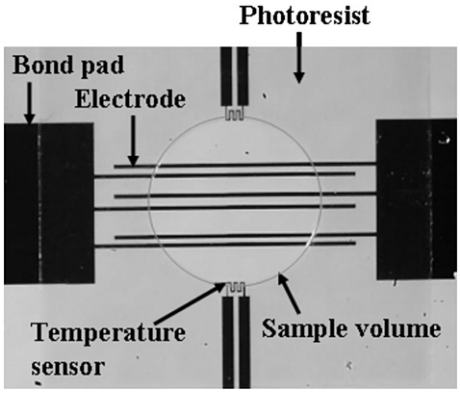

Fig. 3. Electrode glass chip (7×7 mm^2) for EP experiments. The temperature sensor was a platinum meander-structure. A plastic ring in the center of the chamber was fitted to the circular opening in the photoresist to confine the sample volume (7 µl). The chamber was sealed by a cover slip during measurements.

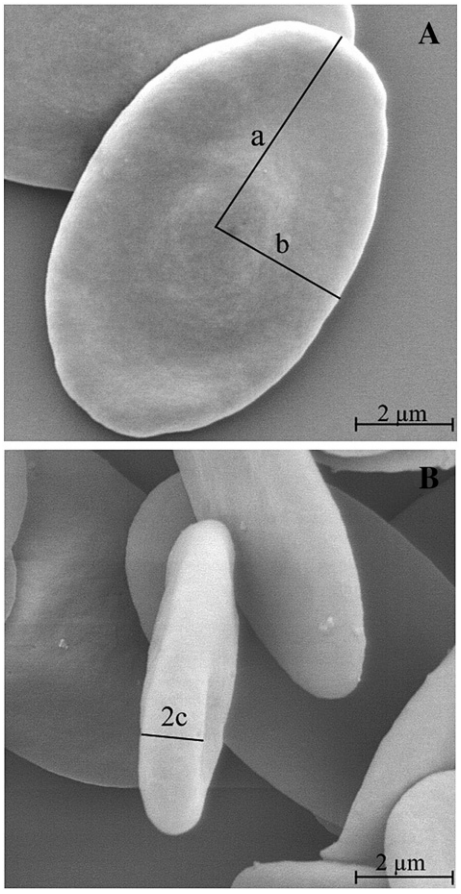

Fig. 4. SEM-micrographs of slightly shrunken CRBCs. (A) and (B) show different orientations of the cells. The semiaxes are denoted (scale bar 2 µm).

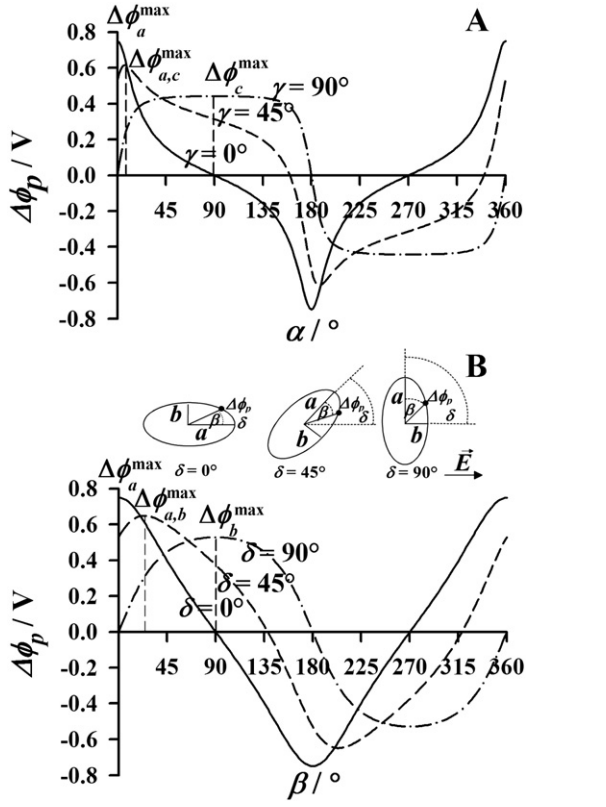

Fig. 5. Angle dependence of $\Delta\phi_p$ for the CRBC model with zero membrane conductance (DC-limit). (A) Dependence of α for peripheral points (β=0°) for a field orientation perpendicular to semiaxis b (δ=0°). Three field orientations (γ=0°, γ=45° and γ=90°) are considered in the a–c plane. (B) Dependence of β for peripheral points (α=0°) for a field orientation perpendicular to semiaxis c (γ=0°). Three field orientations (δ=0°, δ=45° and δ=90°) are considered in the a–b plane.

conductivity was controlled by a conductometer (inoLab, WTW GmbH, Weilheim, Germany) in the temperature compensation mode (20 °C).

3.2.4. EP experiments

PI (Fluka, Switzerland, molecular weight 668.39) binds to DNA and is used as a fluorescence marker of cell nuclei [48]. Cells were suspended in 5 ml measuring solution containing 10 µM PI [36]. 7 µl of this suspension with a cell concentration of 0.03% *v/v* were transferred to the measuring chamber that was sealed by a cover slip. EP experiments were conducted with sedimented cells a few minutes after transfer. The uptake of PI by single cells was observed with a fluorescence microscope (Olympus IX71, Japan). The images were recorded on hard disk and monitored by a computer interface using the Cell-P program of our imaging system (Soft Imaging System GmbH, Germany). Cells already stained before pulse application were excluded from interpretation. EP was judged 3 min after pulse application. Non-lysed cells did not lose their hemoglobin content. PI permeabilized cells detected by fluorescence-staining of their nuclei and non-permeabilized cells were distinguished amongst the non-lysed cells. Data were obtained for 10–15 cells collected in 4–5 repeats for each experimental condition.

4. Results and discussions

4.1. Theoretical analysis

4.1.1. DC-limit of $\Delta\phi_p$ for cells of the general ellipsoidal shape with zero membrane conductance

The following analysis is based on the theoretical descriptions introduced above. Table 1 presents the CRBC parameters used. In the experiments, cells were oriented with semiaxes b or c perpendicular to the external field (Fig. 2A and B). For the first orientation, δ=0° and β=0° for peripheral points in the a–c plane (see Figs. 1 and 2A). The $\Delta\phi_p$ of any point depends on the field angle γ. Maxima at the poles are special cases of Eq. (3) and given for a parallel orientation of the field and semiaxes a ($|\Delta\phi_a^{max}| = a_{infl}\,E$) and c ($|\Delta\phi_c^{max}| = c_{infl}\,E$), respectively. At a field angle of γ=45° (Fig. 2A) Eq. (12) becomes:

$$|\Delta\phi_{a,c}^{max}| = \left(\sqrt{2}/2\right)E\sqrt{a_{infl}^2 + c_{infl}^2} \tag{20}$$

Analogous expressions are obtained for cell orientations in the a–b and b–c planes. It can be shown that the equation holds for cell models with a very thin membrane, zero membrane conductance, and a highly conductive cytoplasm at low frequencies. Under these conditions, the membrane point of $\Delta\phi^{max}$ is solely determined by the object geometry

Table 2
Shape parameters of a spheroidal model for theoretical considerations

Semiaxes	Influential radii calculated from	
	Depolarizing factors	Simplified equations (Appendix A)
Spherical model		
a=b=c=3.5 µm	5.25 µm	5.25 µm
Spheroidal model		
c:a=1:3.5 (oblate)		
a_{infl}=b_{infl}	4.18 µm	4.28 µm
c_{infl}	3.06 µm	2.75 µm
c:a=2:1 (prolate)		
a_{infl}=b_{infl}	5.96 µm	5.83 µm
c_{infl}	8.47 µm	8.75 µm

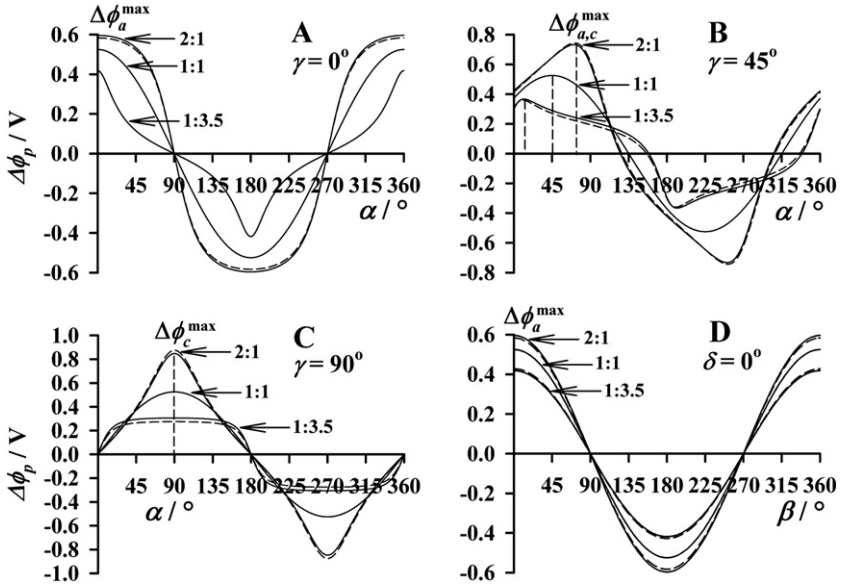

Fig. 6. Comparison of the DC-limits of $\Delta\phi_p$ for the full (Eq. (10), solid lines) and simplified (Eq. (15), dashed lines) spheroidal models. Zero membrane conductance was assumed. (A–C): $\Delta\phi_p$ dependence on α for peripheral membrane points in a–c plane (β=0°) for semiaxis b perpendicular to the field (δ=0°). The field orientations is γ=0° (A), γ=45° (B) and γ=90° (C). (D): trivial case of a field orientation perpendicular to the symmetry axis c (γ=0°, δ=0°). The $\Delta\phi_p$ dependence on β is a cosine function for peripheral membrane points in the a–b plane (α=0°). The $\Delta\phi_p$ magnitude is higher for prolate than for oblate cells.

(see Eq. (11)). We therefore designated the angle of this membrane point "geometry-determined limiting angle". $\alpha_{(\Delta\phi^{max}_{a,c})}$=7.2° is obtained for the geometric parameters of Table 1 (Fig. 5A). $\alpha_{(\Delta\phi^{max}_{a,b})}$ is 23.78° in the a–b plane (Fig. 5B).

4.1.2. DC-limit of $\Delta\phi_p$ of oriented spheroidal cells with zero membrane conductance

We consider the spheroidal shape in the following for the sake of completeness. Semiaxes a and b were fixed to a typical cell value of 3.5 μm. Semiaxis c was varied. Three axes ratios were considered, c:a=1:1 (spherical), c:a=1:3.5 (oblate), and c:a=2:1 (prolate). A field orientation perpendicular to semiaxis b (δ=0°) can be assumed without limitation in generality. $\Delta\phi_p$ of the peripheral membrane points (β=0°) was calculated either by the full model (Eq. (10)) using exact influential radii (Table 2) or by the simplified Eq. (15) (Fig. 6). The $\Delta\phi^{max}$ values were found at the poles of semiaxis a (α=0°) and c (α=90°) for field orientations in parallel (γ=0°, Fig. 6A) and perpendicular (γ=90°, Fig. 6C) to semiaxis a. For γ=45°, $\Delta\phi^{max}$ can be expressed in analogy to

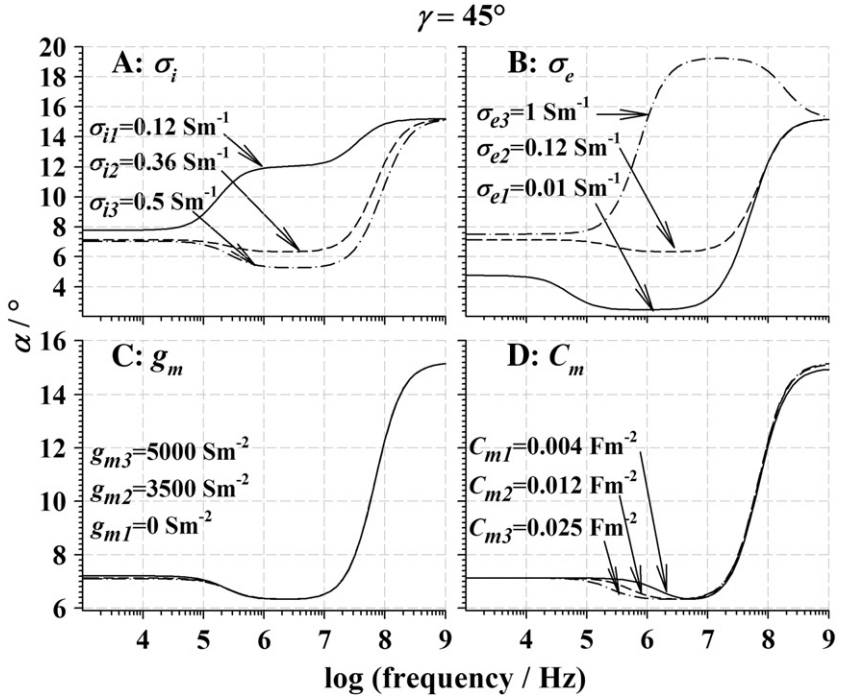

Fig. 7. Frequency dependence of the angle α of the $\Delta\phi^{max}$ membrane point on cell parameters for a field orientation of γ=45° in the a–c plane. (A) internal conductivity, σ_i; (B) external conductivity, σ_e; (C) membrane conductance, g_m; (D) area specific membrane capacitance, C_m.

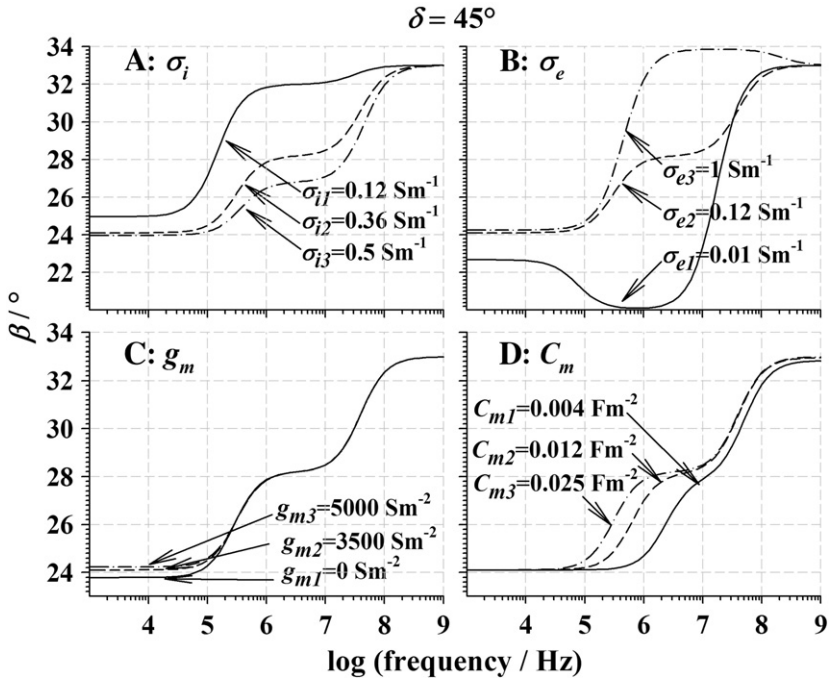

Fig. 8. Frequency dependence of the angle β of the $\Delta\phi^{max}$ membrane point on cell parameters for a field orientation of δ=45° in the *a*–*b* plane. (A) internal conductivity, σ_i; (B) external conductivity, σ_e; (C) membrane conductance, g_m; (D) area specific membrane capacitance, C_m.

Eq. (20) (Fig. 6B). For a field orientation perpendicular to semiaxis *c* (γ=0°), $\Delta\phi^{max}=-a_{inf}E$ for all angles in the *a*–*b* plane (Fig. 6D). The errors of the simplified equations for prolate and oblate shapes are usually much smaller than 10% compared to the full model (Fig. 6).

4.1.3. Dependence of the angle of $\Delta\phi^{max}$ on cell parameters and frequency for tilted cells of the general ellipsoidal shape

The site of $\Delta\phi^{max}$ depends on cell and medium parameters when the object is exposed to the field under a certain angle. For a qualitative consideration we used two different field orientations δ=45° (γ=0°: field in *a*–*b* plane), as well as γ=45° (δ=0°: field in *a*–*c* plane). The effect of cell parameters on the location of $\Delta\phi^{max}$ is considered a function of frequency in Figs. 7 and 8. α and β of the $\Delta\phi^{max}$ membrane points were calculated by Eq. (6). For the iteration of one parameter (σ_e, σ_i, g_m or C_m), all other parameters were kept at their standard values (Table 1). As expected, the angles robustly approaches the geometry-determined limiting angles of 7.2° (*a*–*c* plane, Fig. 7) and 23.78° (*a*–*b* plane, Fig. 8) at low frequencies for a low membrane conductance.

Generally, three frequency plateaus are obtained for the angles. The first and second plateaus occur at frequencies from 0–10^4 Hz and 10^5–10^7 Hz, respectively. While deviations of the first plateau from the geometry-determined limiting angle depend on membrane conductance, especially at low external conductivities, the third (permittivity) plateau is largely independent from the cell parameter variations considered. Only membrane permittivity variations have a slight effect (Figs. 7D and 8D). In contrast, the second plateaus of α and β are strongly affected by the cell parameters. It is interesting, that α and β may be higher or lower than the geometry-determined limiting angle. The reason is that the polarizability balance along the two semiaxes in the field plane may be deflected either to the shorter or the longer semiaxis, i.e. the shorter or the longer semiaxis may be higher polarizable [49]. The plateau levels of α and β are independent of C_m variations. Nevertheless, higher C_m values shift the transition frequency from the first to the second plateaus toward lower frequencies (Figs. 7D and 8D). Please note that the assumption of cell properties varying along the three axis, e.g. of different cytoplasmic permittivities, results in a more complex behavior of the angle of $\Delta\phi^{max}$. Additional transitions and frequency plateaus are obtained for such assumptions (data not shown). Nevertheless, such a situation is realistic for biological cells with non-confocal membranes [47].

The $\Delta\phi$ balance along the three semiaxes is plotted in Fig. 9 to consider the physical background of the angle transitions in Figs. 7 and 8. Fig. 9A shows that the frequency dependence of $\Delta\phi$ is qualitatively very similar along the three semiaxis. At low frequency (< 10^5 Hz) the amplitude of $\Delta\phi$ is frequency independent. The amplitude of $\Delta\phi$ is highest for the longest

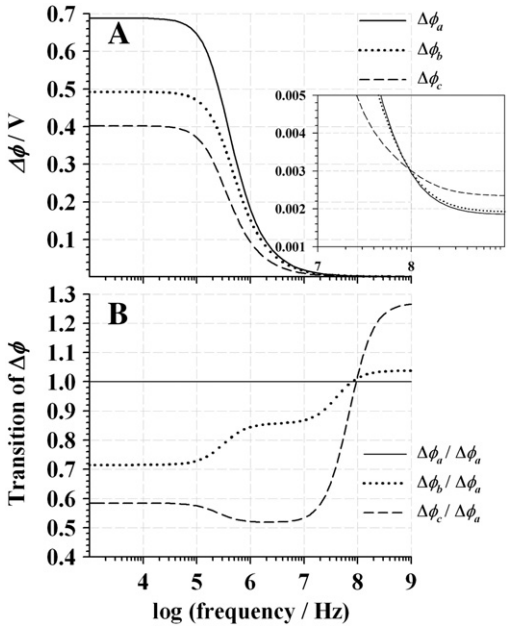

Fig. 9. Frequency dependence of the absolute values of $\Delta\phi$ according to the full model (Eq. (2), Table 1). (A) Frequency dependence of $\Delta\phi$ at the poles for a field orientation along the semiaxes *a*, *b* and *c*, respectively. Insert: curves cross one another at around 100 MHz. (B) amplitudes of $\Delta\phi$ at the poles relative to $\Delta\phi_a$. Please compare to the transitions of $\alpha_{(\Delta\phi^{max})}$ and $\beta_{(\Delta\phi^{max})}$ in Figs. 7 and 8, respectively.

semiaxis ($\Delta\phi_a > \Delta\phi_b > \Delta\phi_c$, Fig. 9A). Transitions of the relative values occur at frequencies above 100 kHz (Fig. 9A). Above 100 MHz the sequence of the magnitudes even reverses ($\Delta\phi_c > \Delta\phi_b > \Delta\phi_a$; Fig. 9A insert, Fig. 9B). The transitions in the relative magnitudes are identical to the transitions of α (compare dashed lines in Fig. 9B to dashed line in Fig. 7) and β (compare dotted lines in Fig. 9B to dashed line in Fig. 8).

4.1.4. Electric field distribution in the EP chamber

We used COMSOL 3.3A Multiphysics program (Comsol AB, Stockholm, Sweden) to consider the three-dimensional electric field distribution in the inter-electrode space of the chip chamber for an electrode height of 100 nm, i.e. the thickness of the platinum layer (Fig. 3). Aqueous solution was assumed to cover both electrodes by 5 µm, the approximate filling height in the EP experiments. The constant field strength found in the center between the electrodes is altered at distances lower than 10 µm to the electrodes. While the field strength is increased close to the chamber bottom ($z<1$ µm) it is decreased for heights of $z=3$ µm and $z=5$ µm at short distances to the electrodes. This is the reason for an increased number of lysed cells in the immediate vicinity of the electrode edges (see cell number 6 in Fig. 10E).

4.2. EP results

4.2.1. Dependence of PI permeabilization and cell lysis of oriented CRBCs on electric field strength, frequency and pulse duration

CRBCs are nucleated and have a three-axial ellipsoidal shape. The nuclei are clearly visible (Figs. 4 and 10). The semiaxes measures obtained from 60 cells were $a{:}b{:}c = 6.66 \pm 0.19$ µm: 4.17 ± 0.26 µm:1.43 ± 0.08 µm. Experimental considerations were restricted to the case of semiaxis c being perpendicularly oriented to the external field $\boldsymbol{E}$ ($\gamma=\alpha=0°$; see also Fig. 2B). Fig. 10 presents examples of phase-contrast and fluorescence micrographs of CRBCs immediately and 3 min after the pulse. Three

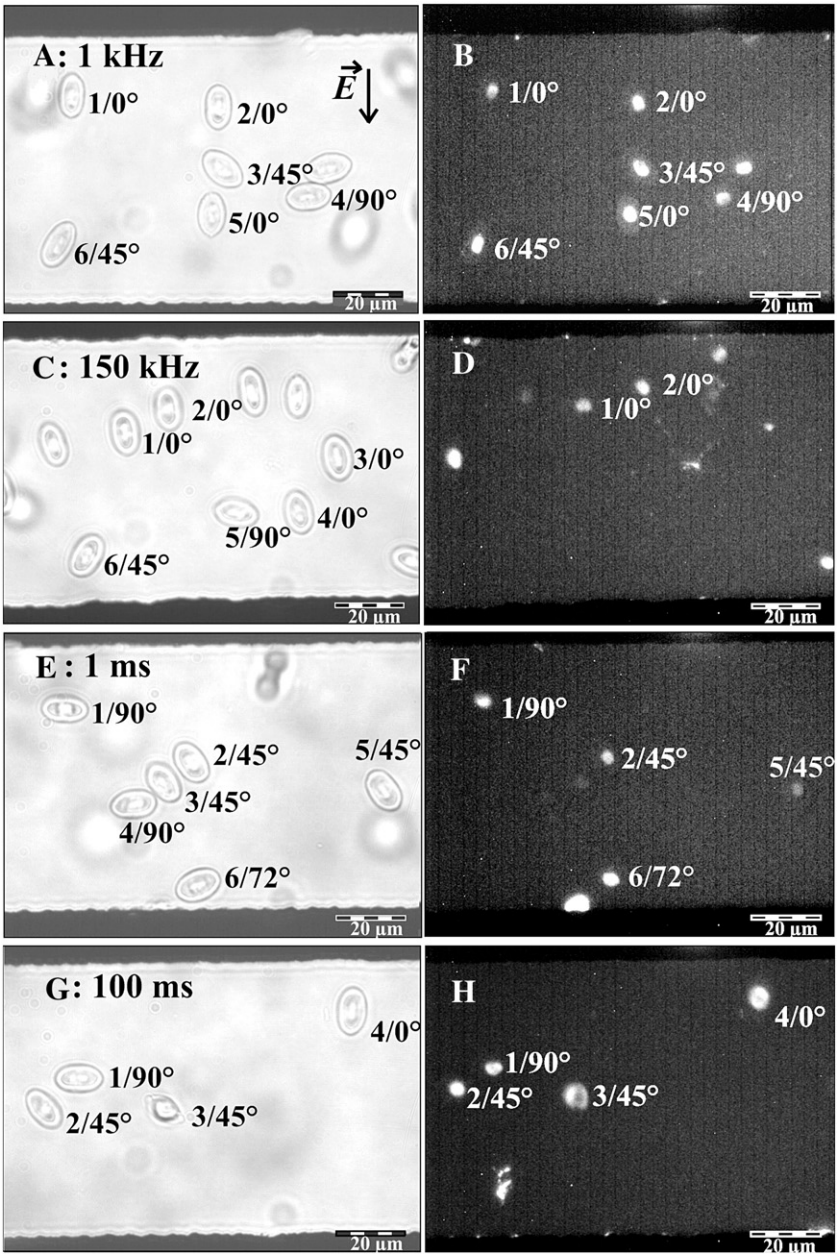

Fig. 10. EP of oriented CRBCs suspended in 10 µM PI solution ($\sigma_e = 0.12$ S m^{-1}). Left column (A, C, E and G): phase contrast micrographs immediately after the pulse. Right column (B, D, F and H): fluorescence micrographs 3 min after pulses of $E = 200$ kV m^{-1} (16 V_{pp}, electrode distance 80 µm). Different pulse durations of 1 ms (E), 10 ms (A and C) and 100 ms (G) as well as different field frequencies of 1 kHz (A, E and G) and 150 kHz (C) were used. Cell numbers and the orientation angles of their semiaxes a with respect to the field are indicated. PI permeabilized (small fluorescent spots, normal nucleus size) and lyzed (E: number 6, G: numbers 3 and 4, swollen nuclei) cells were distinguished from the appearance of their nuclei.

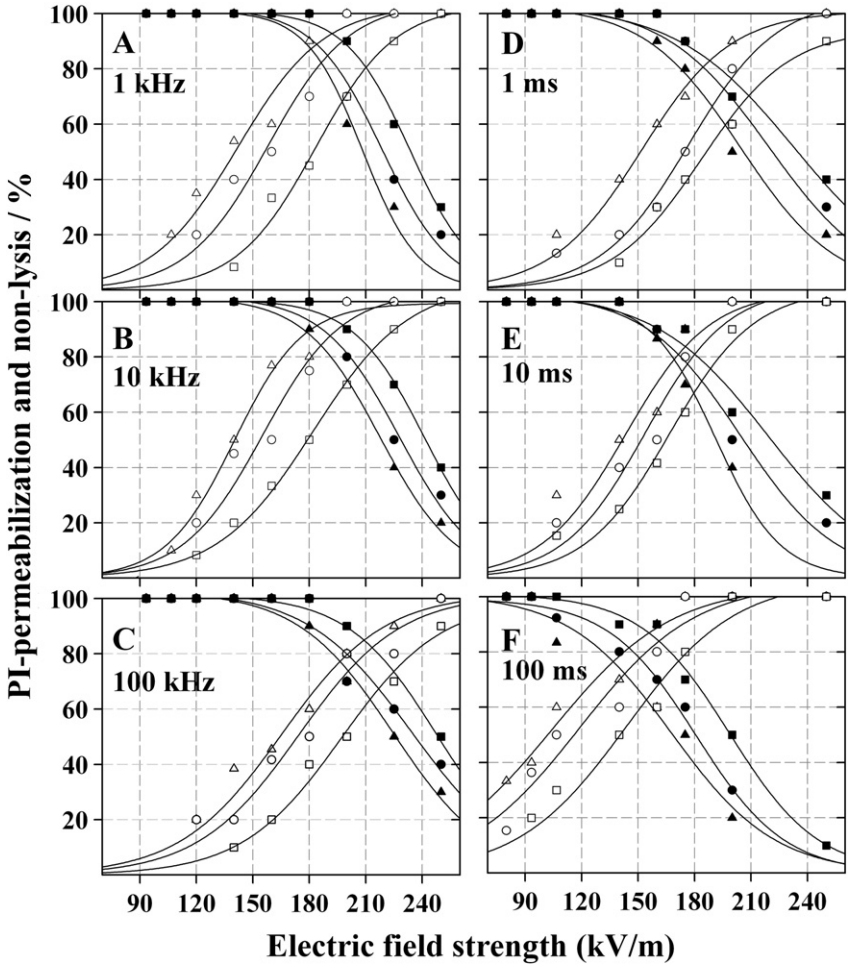

Fig. 11. Field strength dependence of PI permeabilization and survival (non-lysis) of CRBCs for selected field frequencies (A–C) and pulse durations (D–F) at σ_e=0.12 S m^{-1}. Pulse duration was 10 ms (A–C). Field frequency was 1 kHz (D–F). Cell orientations of δ=0° (triangles), 45° (circles), and 90° (squares) were considered. Hollow and filled symbols indicate the percentages of PI permeabilization and non-lysis, respectively. Sigmoidal curves (Eq. (21)) were fitted to the measuring points.

angle-classes of cell orientation were considered as indicated in Fig. 10 (δ=0°, 45° and 90°).

Frequency dependence of EP: the pulse duration was kept constant at 10 ms to consider the frequency dependence. Examples are shown in Fig. 10A–D. Cells of all orientations were permeabilized for PI at 1 kHz (Fig. 10A and B). Only cells oriented parallel to the field (cells 1 and 2) were permeabilized for PI at 150 kHz, while cells oriented at 45° and 90° (cells 5 and 6) were not permeabilized (Fig. 10C and D). Detailed results on the frequency dependence are given in Fig. 11A–C.

Pulse duration dependence of EP: the frequency was kept constant at 1 kHz to consider the pulse duration dependence. Examples are shown in Fig. 10E–H. Four out of six cells were permeabilized for PI at 1 ms (Fig. 10E and F). All cells were permeabilized for PI by the longer 100 ms pulse. Two cells even lysed (cells 3 and 4 in Fig. 10G and H). Lysed cells lost their hemoglobin content after pulse application, their nuclei swelled. An example is cell number 6 in Fig. 10E. For its location close to the electrode, it is the only lysed cell, even though it is oriented at 72°. Detailed results of the pulse duration dependence are given in Fig. 11D–F.

The percentages of PI permeabilized and non-lysed cells were plotted over field strength for different pulse durations and field frequencies to analyze the electroporation properties of CRBCs. Sigmoidal curves were fitted to the experimental data (Fig. 11):

$$y = \frac{a}{1 + \exp((E_{50\%} - E)/b)} \tag{21}$$

Where *y*, *a*, and *b* denote the percentages of cells complying with one of the two criteria (PI permeabilization or non-lysis), the final (*b* negative) or starting (*b* positive) percentage of cells for zero-field strength and the slope of the sigmoidal curve. *E* is the electric field strength of a data point and $E_{50\%}$ determines the electric field strength corresponding to the 50% criterion [13,50]. All curves were fitted using a nonlinear least-square regression program (SigmaPlot 9.5). Fig. 11 show results of the frequency, pulse length, field strength and orientation dependencies for the two criteria [11–15,17].

Fig. 11A–C present selected results for the frequency dependence for a constant pulse duration of 10 ms. The figure shows a higher EP efficiency at lower frequencies (compare to Gimsa and Wachner [29]).

Fig. 11D–F present selected results for the effect of pulse duration for a constant frequency of 1 kHz. This frequency is low enough to be still in the plateau range of the DC-limit (Fig. 9) and high enough to avoid electrode effects. Higher field strengths are required for an effective EP at shorter pulse durations and higher numbers of lysed cells are found at longer pulse durations [14,15]. Clearly, EP efficiency is higher at a cell orientation of δ=0° than at δ=45° and 90° [23].

4.2.2. Critical field strength for oriented cells in dependence of field frequency and pulse duration

We defined critical field strengths E_{crit} for PI permeabilization and cell lysis from the 50%-values of the fitted curves in Fig. 11, i.e. 50% of the cells comply with one of the criteria at E_{crit} [1]. The E_{crit} for PI permeabilization was always lower than for cell lysis independent of cell orientation.

Fig. 12 presents the frequency and pulse duration dependence of the two E_{crit} parameters. The parameters increase for higher frequencies (Fig. 12A) and shorter pulses (Fig. 12B). Below 100 kHz

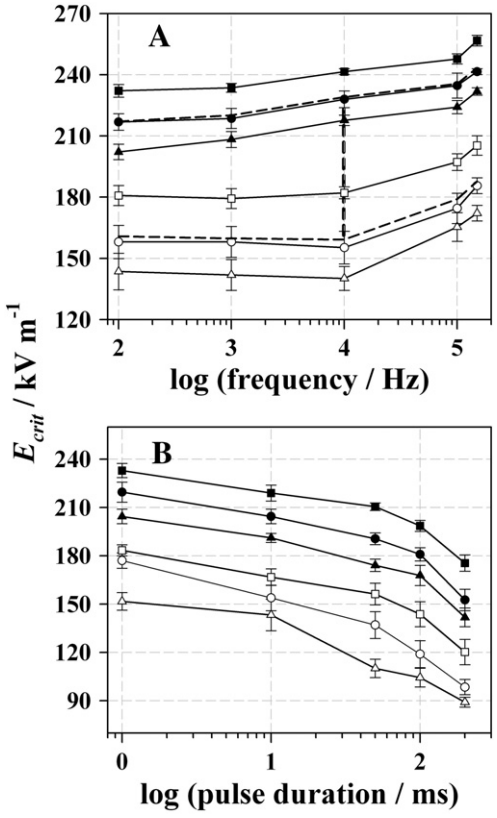

Fig. 12. Comparison of E_{crit} for PI permeabilization and non-lysis for various field frequencies (A, const. pulse duration of 10 ms) and pulse durations (B, const. field frequency of 1 kHz). Three cell orientations are considered. Dashed lines in (B) denote the average of the orientations for the two E_{crit} criteria. The dotted vertical line marks the optimal frequency for differentiation of PI permeabilization and non-lysis.

the E_{crit} for PI permeabilization was independent of frequency, whereas it is increasing at higher frequencies [22]. This behavior is in accordance with Eqs. (4) and (5). Nevertheless, E_{crit} for cell non-lysis increases linearly with frequency also below 100 kHz (Fig. 12A). The reason may be that the nonlinear processes related to the formation of large aqueous pores, membrane rupture, and cell lysis are much stronger than those resulting in PI permeabilization [7–9]. Further, the different relations of the E_{crit} values for PI permeabilization and cell non-lysis (Table 3) at the different angles of cell orientation are most probably resulting from these properties. Our model does not describe complex changes of the membrane properties during the process of pore formation and membrane rupture. For these reasons, no $\Delta\phi_{crit}$ values were derived from the cell lysis data.

A field frequency of 10 kHz was chosen to search for the optimal pulse duration. This frequency is high enough to exclude electrode processes and at the same time still below the membrane dispersion. Averaging over all cell orientations led to mean values of E_{crit} for the two parameters PI permeabilization and cell lysis in dependence on frequency (dashed lines in Fig. 12A). The criterion for the optimal pulse duration was high PI permeabilization at low cell lysis. The distances between the average lines are frequency dependent, suggesting an optimal differentiation of the two criteria at a pulse duration of 10 ms (dotted vertical line in Fig. 12A). The field oscillates 100 times at this relatively short pulse duration.

$\Delta\phi_{crit}$ values could be obtained from E_{crit} by fitting the respective summands of Eq. (4) using the parameters of Table 1 (Fig. 13; see also Marszalek et al. [22]). Field orientations of δ=0° (first summand of Eq. (4) for $d_x=a$), δ=90° (second summand of Eq. (4), $d_y=b$) and δ=45° (both summands of Eq. (4)) were considered. While the angles of $\Delta\phi^{max}$ are frequency independent for δ=0° and 90° (β equal to δ), $\Delta\phi^{max}$ shows a complex behavior for δ=45° (Fig. 8). Nevertheless, this complex behavior appears beyond our experimental frequency range (Fig. 13). For this reason, we neglected the membrane conductance and used the geometry determined limiting angle (compare to Eq. (11)) to calculate $\Delta\phi_{crit}$ from the determined E_{crit} values (Fig. 12A). The obtained $\Delta\phi_{crit}$ values for PI permeabilization are given in Table 3. Theoretical $\Delta\phi_{crit}$ values were only calculated for PI permeabilization for the reasons discussed above.

Fig. 13 presents the frequency dependence of PI permeabilization. The low deviation of the curves from the data points indicates that the cell parameters of Table 1 are reasonable assumptions for CRBCs. The assumption of a specific membrane capacitance even higher than 0.025 F m^{-2} (Table 1) would probably result in a theoretical E_{crit} increase already at lower frequencies and improved fits at higher frequencies (see also [47]). Nevertheless, other probe molecules may yield different values.

Our results confirm that the membrane sensitivity toward the field depends on membrane curvature. Three factors may be important for this effect: i) the larger the area oriented perpendicularly to the field (low curvature) the larger the area experiencing a high $\Delta\phi$ and the higher the probability of pore formation. As a result the membrane sensitivity for the induced $\Delta\phi$ will be higher along the two shorter semiaxes; ii) the surface tension generates forces attracting membrane molecules from other membrane areas. These forces are stronger in areas of higher curvature around the poles of the longer axis, i.e. when molecules are becoming available by the growth of pores they are faster collected in areas of high curvature leading to a facilitated pore growth in areas of low curvature. Nevertheless, such a global effect may require a membrane property that provides argument iii): areas of higher curvature may be stabilized by molecular structures near the poles of the longer semiaxis. As a result, the membrane will be less sensitive toward field-induced distortions in these areas. In practice, a combination of the above and

Table 3
Comparison of critical field strengths (E_{crit}) and critical $\Delta\phi$ ($\Delta\phi_{crit}$) for PI permeabilization for different orientations of semiaxis a with respect to the field

Parameter	Cell orientations		
	0°	45°	90°
E_{crit}/kV m^{-1} (PI permeabilization, 1 kHz, 10 ms)	141.89±7.53	158.07±7.59	179.34±4.88
E_{crit} relative to E_{crit} at 0°	1	1.11	1.26
E_{crit}/kV m^{-1} (non-lysed cells, 1 kHz, 10 ms)	208.29±3.93	218.59±4.89	233.59±2.16
E_{crit} relative to E_{crit} at 0°	1	1.05	1.12
$\Delta\phi_{crit}$/V (theoretical analysis of data in Fig. 13)	0.99	0.94	0.89
$\Delta\phi_{crit}$ relative to $\Delta\phi_{crit}$ at 0°	1	0.95	0.89

Please note that E_{crit} for PI permeabilization for a field rotating in the a–b plane was approx. 115 kV m^{-1} corresponding to a $\Delta\phi_{crit}$ of 0.79 V at 0°.

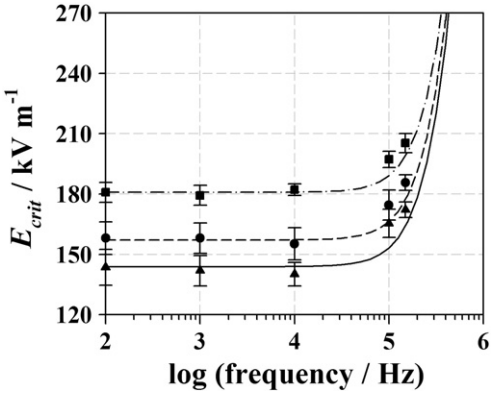

Fig. 13. Fitted frequency dependencies of E_{crit} of PI permeabilization for three cell orientations over frequency (data of Fig. 12A). Eqs. (4) and (5) and the parameters of Table 1 were used. The fits yielded the $\Delta\phi_{crit}$-values of Table 3.

other unknown effects may explain our findings. Please also note, that the actual curvatures in CRBCs are different from those of a general ellipsoid of the same axis-lengths (Fig. 4).

5. Conclusions

We developed a model for the $\Delta\phi$ induced in three-axial ellipsoidal and spheroidal cells with an arbitrary orientation within the field in order to analyze the effects of cell orientation, field strength and frequency. The model was tested in EP experiments on ellipsoidal CRBCs of different orientations in a glass chip chamber. The chamber provided homogeneous fields in large areas between the electrodes. The permeabilization and lysis rates were only increased for cells sedimented in the immediate vicinity of the electrodes due to the strongly inhomogeneous fields at these sites. Integrated temperature sensors allowed us to prove that the EP pulse did not induce a strong temperature increase in the chamber.

The percentages of PI permeabilized and lysed cells increased with pulse duration and decreased with field frequency. The optimal pulse duration and field frequency, i.e. a high percentage of PI permeabilization at a low lysis rate, were approx. 10 ms and 10 kHz for CRBCs at an external conductivity of 0.12 S m^{-1}. Theoretical analysis showed that $\Delta\phi$ is highest when the longest semiaxis is oriented in parallel to the field. This is expressed in the lowest E_{crit} values for PI permeabilization (142 kV m^{-1}) and cell lysis (208 kV m^{-1}) at this orientation. Nevertheless, model analysis revealed that $\Delta\phi_{crit}$ for PI permeabization was different along the *a*- (δ=0°, 0.99 V) and *c*-axes (δ=90°, 0.89 V) and for the intermediate orientation (δ=45°, 0.94 V) [22]. Possible reasons for this higher field sensitivity of membrane areas with lower curvature are discussed. Comparison of the lowest E_{crit} for PI staining in a linear field (142 kV m^{-1}) and a field rotating in the *a*–*b* plane (115 kV m^{-1}) revealed the higher EP efficiency of rotating fields.

Theoretically, the location of the $\Delta\phi^{max}$ membrane point in DC or low frequency fields depends on cell parameters in the event that the field is not oriented parallel to one of the axes. Its location changes with frequency in the dispersion ranges of cell polarization. For an arbitrary field angle, the $\Delta\phi^{max}$ point will exhibit a complex frequency-dependent trajectory at the membrane surface.

Acknowledgements

KM is grateful for a stipend from the Royal Thai government. This study has partly been supported by grant StSch 20020418A of the Bundesamt für Strahlenschutz to JG. The authors are grateful to the International Postgraduate Program (IPP) supported by DAAD, BMBF and DFG. We would like to thank C. Tautorat and Dr. W. Kröger for their help with the chip carriers, as well as M. Stubbe for help with the COMSOL Multiphysics program. J. Donath is acknowledged for technical assistance and R. Sleigh for help with the manuscript. We also thank Prof. Dr. L. Jonas from the Electron Microscopy Centre of the Medical Faculty, University of Rostock for the SEM micrographs.

Appendix A

Simplified equations of the influential radius for spheroidal cells

The plot of the relative influential radius a_{infl}/a compared to the logarithm of the axis ratio exhibits a sigmoidal shape for spheroids (see [46] for more details). This behavior can be approximated by:

$$\frac{a_{infl}}{a} = \frac{a+2c}{a+c} = 2 - \frac{1}{1+(c/a)} \tag{A1}$$

The limiting values for infinitely thin disks, spheres and infinitely long cylinders 1, 1.5, and 2 are correctly reflected by Eq. (A1). Since the sum of the depolarizing factors (n_a+n_b+n_c) along the three principal axes of a general ellipsoid is always unity [51,52] it follows that $a/a_{infl}+b/b_{infl}+c/c_{infl}=2$ [49] and for the relative influential radius c_{infl}/c along the symmetry axis *c*:

$$\frac{c_{infl}}{c} = \frac{a+2c}{2c} = 1 + \frac{1}{2(c/a)} \tag{A2}$$

References

[1] E. Neumann, A. Sprafke, E. Boldt, H. Wolf, Biophysical considerations of membrane electroporation, in: D.C. Chang, B.M. Chassy, J.A. Saunders, A.E. Sowers (Eds.), Guide to electroporation and electrofusion, Academic Press, San Diego, 1992, pp. 77–90.
[2] K. Kinosita Jr., T.Y. Tsong, Voltage-induced pore formation and hemolysis of human Erythrocytes, Biochim. Biophys. Acta 471 (1977) 227–242.
[3] A.J.H. Sale, W.A. Hamilton, Effects of high electric fields on microorganisms III. Lysis of erythrocytes and protoplasts, Biochim. Biophys. Acta 163 (1968) 37–43.
[4] U. Zimmermann, The effect of high intensity electric field pulses on eukaryotic cell membranes: fundamentals and applications, in: U. Zimmermann, G.A. Neil (Eds.), Electromanipulation of Cells, CRC, Boca Raton, FL, 1996, pp. 1–106.
[5] J. Teissie, M.P. Rols, An experimental evaluation of the critical potential difference inducing cell membrane electropermeabilization, Biophys. J. 65 (1993) 409–413.
[6] U. Zimmermann, R. Benz, Dependence of the electrical breakdown voltage on the charging time in *Valonia utricularis*, J. Memb. Biol. 53 (1980) 33–43.
[7] R.W. Glaser, S.L. Leikin, L.V. Chernomordik, V.F. Pastushenko, A.I. Sokirko, Reversible electrical breakdown of lipid bilayers: formation and evolution of pores, Biochim. Biophys. Acta 940 (1988) 275–287.
[8] R.W. Glaser, J. Gimsa, Gradual changes of membrane properties at high transmembrane electric potential simulate a breakdown threshold, in: M. Blank (Ed.), Electricity and magnetism in biology and medicine, San Francisco Press, Inc., San Francisco, 1993, pp. 135–137.
[9] L.V. Chernomordik, S.I. Sukharev, S.V. Popov, V.F. Pastushenko, A.V. Sokirko, I.G. Abidor, Y.A. Chizmadzhev, The electrical breakdown of cell and lipid membranes: the similarity of phenomenologies, Biochim. Biophys. Acta 902 (1987) 360–373.
[10] R. Benz, U. Zimmermann, High electric field effects on the cell membranes of *Halicystis parvula*: A charge pulse study, Planta 152 (1981) 314–318.
[11] A.M. Lebar, D. Miklavcic, Cell electropermeabilization to small molecules *in vitro*: control by pulse parametes, Radiol. Oncol. 35 (2001) 193–202.
[12] K.J. Müller, V.L. Sukhorukov, U. Zimmermann, Reversible electropermeabilization of mammalian cells by high-intensity, ultra-short pulses of submicrosecond duration, J. Membr. Biol. 184 (2001) 161–170.
[13] M. Puc, T. Kotnik, L.M. Mir, D. Miklavcic, Quantitative model of small molecules uptake after in vitro cell electropermeabilization, Bioelectrochemistry 60 (2003) 1–10.
[14] M.P. Rols, J. Teissie, Electropermeabilization of mammalian cells: quantitative analysis of the phenomenon, Biophys. J. 58 (1990) 1089–1098.
[15] M.P. Rols, J. Teissie, Electropermeabilization of mammalian cells to macromolecules: Control by pulse duration, Biophys. J. 75 (1998) 1415–1423.
[16] J. Teissie, C. Ramos, Correlation between electric field pulse induced long-lived permeabilization and fusogenicity in cell membranes, Biophys. J. 74 (1998) 1889–1898.
[17] H. Wolf, M.P. Rols, E. Boldt, E. Neumann, J. Teissie, Control by pulse parameters of electric field-mediated gene transfer in mammalian cells, Biophys. J. 66 (1994) 524–531.
[18] D. Fologea, T.V. Dimov, I. Stoica, O. Csutak, M. Radu, Increase of Saccharomyces cerevisiae plating efficiency after treatment with bipolar electric pulses, Bioelectrochem. Bioenerg. 46 (1998) 285–287.
[19] T. Kotnik, L.M. Mir, K. Flisar, M. Puc, D. Miklavcic, Cell membrane electropermeabilization by symmetrical bipolar rectangular pulses: Part I. Increased efficiency of permeabilization, Bioelectrochemistry 54 (2001) 83–90.
[20] T. Kotnik, G. Pucihar, M. Rebersek, D. Miklavcic, L.M. Mir, Role of pulse shape in cell membrane electropermeabilization, Biochim. Biophys. Acta 1614 (2003) 193–200.
[21] H.G.L. Coster, U. Zimmermann, The mechanism of electrical breakdown in the membranes of *Valonia utricularis*, J. Memb. Biol. 22 (1975) 73–90.
[22] P. Marszalek, D.S. Liu, T.Y. Tsong, Schwan equation and transmembrane potential induced by alternating electric field, Biophys. J. 58 (1990) 1053–1058.
[23] B. Valic, M. Golzio, M. Pavlin, A. Schatz, C. Faurie, B. Gabriel, J. Teissie, M.P. Rols, D. Miklavcic, Effect of electric field induced transmembrane potential on spheroidal cells: theory and experiment, Eur. Biophys. J. 32 (2003) 519–528.
[24] H. Fricke, The electric permittivity of a dilute suspension of membrane-covered ellipsoids, J. Appl. Phys. 24 (1953) 644–646.
[25] J. Gimsa, D. Wachner, On the analytical description of transmembrane voltage induced on spheroidal cells with zero membrane conductance, Eur. Biophys. J. 30 (2001) 463–466.
[26] D.C. Chang, J.R. Hunt, Q. Zheng, P.Q. Gao, Electroporation and electrofusion using a pulsed radio-frequency electric field, in: D.C. Chang, B.M. Chassy, J.A. Saunders, A.E. Sowers (Eds.), Guide to electroporation and electrofusion, Academic Press, San Diego, 1992, pp. 303–326.
[27] J. Bernhardt, H. Pauly, On the generation of potential differences across the membranes of ellipsoidal cells in an alternating electrical field, Biophysik 10 (1973) 89–98.
[28] G. Fuhr, R. Hagedorn, R. Glaser, J. Gimsa, T. Müller, Membrane potentials induced by external rotating electrical fields, J. Bioelectr. 6 (1987) 49–69.
[29] J. Gimsa, D. Wachner, A unified resistor–capacitor model for impedance, dielectrophoresis, electrorotation, and induced transmembrane potential, Biophys. J. 75 (1998) 1107–1116.

[30] J. Gimsa, D. Wachner, Analytical description of the transmembrane voltage induced on arbitrarily oriented ellipsoidal and cylindrical cells, Biophys. J. 81 (2001) 1888–1896.
[31] C. Grosse, H.P. Schwan, Cellular membrane potentials induced by alternating fields, Biophys. J. 63 (1992) 1632–1642.
[32] E. Neumann, The relaxation hysteresis of membrane electroporation, in: E. Neumann, A.E. Sowers, C.A. Jordan (Eds.), Electroporation and electrofusion in cell biology, Plenum Press, New York, 1989, pp. 61–82.
[33] H.P. Schwan, Biophysics of the interaction of electromagnetic energy with cells and membranes, in: M. Grandolfo, S.M. Michaelson, A. Rindi (Eds.), Biological effects and dosimetry of nonionizing radiation, Plenum Press, New York, 1983, pp. 213–231.
[34] T.Y. Tsong, Electroporation of cell membranes: mechanism and applications, in: E. Neumann, A.E. Sowers, C.A. Jordan (Eds.), Electroporation and electrofusion in cell biology, Plenum Press, New York, 1989, pp. 149–163.
[35] J. Gimsa, E. Donath, R. Glaser, Evaluation of the data of simple cells by electrorotation using square-topped fields, Bioelectrochem. Bioenerg. 19 (1988) 389–396.
[36] J. Gimsa, P. Marszalek, U. Loewe, T.Y. Tsong, Electroporation in rotating electric fields, Bioelectrochem. Bioenerg. 29 (1992) 81–89.
[37] Y. Huang, B. Rubinsky, Micro-electroporation: improving the efficiency and understanding of electrical permeabilization of cells, Biomed. Microdevices 2 (1999) 145–150.
[38] Y. Huang, B. Rubinsky, Microfabricated electroporation chip for single cell membrane permeabilization, Sens. Actuator A 89 (2001) 242–249.
[39] Y. Huang, B. Rubinsky, Flow-through micro-electroporation chip for high efficiency single-cell genetic manipulation, Sens. Actuator A 104 (2003) 205–212.
[40] Y.C. Lin, M.Y. Huang, Electroporation microchips for *in vitro* gene transfection, J. Micromech. Microeng. 11 (2001) 542–547.
[41] Y.C. Lin, M. Li, C.S. Fan, L.W. Wu, A microchip for electroporation of primary endothelial cells, Sens. Actuator A 108 (2003) 12–19.
[42] Y.C. Lin, M. Li, C.C. Wu, Simulation and experimental demonstration of the electric field assisted electroporation microchip for *in vitro* gene delivery enhancement, Lab Chip 4 (2004) 104–108.
[43] J.A. Kim, K. Cho, Y.S. Shin, N. Jung, C. Chung, J.K. Chang, A multi-channel electroporation microchip for gene transfection in mammalian cells, Biosens. Bioelectron. 22 (2007) 3273–3277.
[44] H. Lu, M.A. Schmidt, K.F. Jensen, A microfluidic electroporation device for cell lysis, Lab Chip 5 (2005) 23–29.
[45] J. Gimsa, D. Wachner, A polarization model overcoming the geometric restrictions of the Laplace solution for spheroidal cells: obtaining new equations for field-induced forces and transmembrane potential, Biophys. J. 77 (1999) 1316–1326.
[46] K. Maswiwat, D. Wachner, R. Warnke, J. Gimsa, Simplified equations for the transmembrane potential induced in ellipsoidal cells of rotational symmetry, J. Phys. D: Appl. Phys. 40 (2007) 914–923.
[47] S. Lippert, J. Gimsa, High resolution measurements of dielectric cell properties by a combination of AC-electrokinetic effects, in: P. Kostarakis (Ed.), Proc. 2nd Inernational Workshop on Biological Effects of EMFs, Rhodes, Greece, 2002, pp. 830–836.
[48] C.J.G. Yeh, B.L. His, W.P. Faulk, Propidium iodide as a nuclear marker inimmuno-fluorescence. II. Use with cellular identification and viability studies, J. Immunol. Methods 43 (1981) 269–275.
[49] J. Gimsa, A comprehensive approach to electro-orientation, electrodeformation, dielectrophoresis, and electrorotation of ellipsoidal particles and biological cells, Bioelectrochemistry 54 (2001) 23–31.
[50] G. Pucihar, T. Kotnik, M. Kanduser, D. Miklavcic, The influence of medium conductivity on electropermeabilization and survival of cells in vitro, Bioelectrochemistry 54 (2001) 107–115.
[51] J.A. Stratton, Electromagnetic theory, McGraw-Hill, New York, 1941.
[52] U. Stille, Der Entmagnetisierungsfaktor und Entelektrisierungsfaktor für Rotation-sellipsoide, Archiv Elektrotechnik 38 (1944) 91–101 (in German).